

# Macrodiversity Power Control in Hierarchical CDMA Cellular Systems

John Y. Kim, *Student Member, IEEE*, Gordon L. Stüber, *Fellow, IEEE*, and Ian F. Akyildiz, *Fellow, IEEE*

**Abstract**—Hierarchical code division multiple access (CDMA) cellular systems, consisting of macrocells with underlying microcells, are studied. We seek power control schemes which will allow both hierarchical layers to share the same spectrum. For the reverse link, hierarchical maximal ratio combining (HMRC) is applied where each mobile station (MS) is received and coherently combined by base stations (BSs) in both layers. For the forward link, selective transmit diversity (STD) is applied where each BS provides multiple transmit paths for MSs to choose. We show that both HMRC and STD are effective in hierarchical CDMA architectures. We conclude that hierarchical architectures are a viable solution for improving CDMA cellular system capacity, and a significant performance gain can be achieved without assigning disjoint spectrum between the layers, by utilizing macrodiversity schemes such as HMRC and STD.

**Index Terms**—Hierarchical cellular architectures, macrodiversity, maximal ratio combining, power control, selective transmit diversity.

## I. INTRODUCTION

**F**UTURE cellular systems will most likely employ a hierarchical architecture consisting of macrocells with underlying microcells. Such hierarchical architectures are of great interest since they can boost system capacity on a per-need basis. In such architectures, macrocells cover large areas with sparse traffic densities, whereas microcells serve small areas with high-traffic densities. However, due to their effective frequency reuse factor of one, hierarchical code division multiple access (CDMA) systems still must deal with cross-interference between the hierarchical layers. This cross-layer interference can be subdued by assigning a distinct spectrum to each layer, but such methods make inefficient use of the already scarce wireless spectrum. Several studies have been performed on hierarchical CDMA settings [1]–[3], none of which suggests any effective power control scheme nor provides the detailed capacity analysis for such architectures, although [1] does suggest a moderate capacity gain when umbrella macrocell(s) are sparsely loaded compared to the embedded microcell(s). This paper proposes schemes that allow hierarchical layers to share the same spectrum, yet achieve a high capacity/performance gain. We generalize our analysis in terms of individual cell loads and do not assume any particular system loading patterns.

For the reverse link, we apply a scheme called hierarchical maximal ratio combining (HMRC), where the signal from each

mobile station (MS) is received by several base stations (BSs) in both hierarchical layers and coherently combined. If we assume independent interference at different BS locations, the combined carrier-to-interference ratio (CIR) is the algebraic sum of the CIRs at each BS

$$\text{CIR}_{\text{HMRC}} = \sum_{i=1}^N \text{CIR}_{\text{micro}i} + \sum_{j=1}^M \text{CIR}_{\text{macro}j} \quad (1)$$

where  $N$  and  $M$  are the number of BSs involved in combining. Recently, macrodiversity MRC (MMRC) has been proven to be an effective way of improving the capacity in cellular CDMA systems [4], [5]. In [4], the author proved the existence of a power control solution using MMRC and showed that the capacity is unaffected by outside interference. In [5], by assuming equal reverse interference level at each BS in nonhierarchical settings, the authors constructed a simple proof showing that MMRC reverse link capacity is close to an isolated-cell capacity. We further generalize the results in [5] and apply them to our hierarchical CDMA model. We derive an analytical solution for HMRC reverse performance without assuming equal level of reverse-link interference among cells and show that both microcell and macrocell performances are nearly unaffected by each other's presence.

The reverse link is commonly considered to limit the CDMA system capacity. However, with the emergence of asymmetric wireless data services, the forward-link performance is becoming increasingly important. For the forward link, HMRC-like combining schemes are not suitable because such schemes will increase the forward-link interference [6]. Instead, we apply a selective transmit diversity (STD) technique where each BS provides multiple transmit paths by means of spatially separated antennas, and the system allows each MS to connect to the most robust path among the multiple paths [7], [8]. Our forward power control law is based on the neighboring-cell pilot power (NPP) scheme proposed in [6], where the forward transmit power to each MS is determined according to link conditions between the MS and surrounding BSs (see Appendix A). For a single macrocell–microcell model

$$P_{\text{cell}} = \frac{G_{\text{micro}} + (1/\gamma)G_{\text{macro}}}{G_{\text{cell}}} \quad (2)$$

where  $\gamma$  is the ratio between the microcell and macrocell total forward transmit powers. While NPP does not offer any significant performance gain over conventional power control schemes, it does guarantee that every MS experiences the same forward-CIR level. Unlike other CDMA forward power control analysis in [9] and [10], our analysis is fully verified by Monte

Manuscript received August 15, 1999; revised April 15, 2000. This research was supported by Korea Telecom Access Network Research Laboratory.

The authors are with the School of Electrical and Computer Engineering, Georgia Institute of Technology, Atlanta, GA 30332-0250 USA (e-mail: ykim@ece.gatech.edu; stuber@ece.gatech.edu; ian@ece.gatech.edu).

Publisher Item Identifier S 0733-8716(01)00120-2.

Carlo simulation. We show that STD is a viable option for hierarchical CDMA forward power control.

We note that, with macrodiversity, there is no longer a clear distinction of cell boundaries among cells and layers. Therefore, readers should be aware that MSs are referenced to their respective locations. For example, a microcell MS means that the MS is physically located in the designated microcell area, not necessarily served by it.

The remainder of the paper is organized as follows. In Section II, our system models are described and the corresponding analytical solutions are derived. Our simulation results, including the performance comparison with non-HMRC and non-STD schemes, are presented in Section III. Finally, the paper is concluded with some final remarks in Section IV.

## II. SYSTEM MODEL AND ANALYSIS

Our hierarchical model consists of a group of overlaying omnidirectional macrocells and a cluster of omnidirectional microcells embedded within the macrocells. We assume that the MSs are uniformly distributed in both macrocells and microcells, yet the load condition of each cell might differ. Although we do not assume any particular load conditions, microcells are generally more densely populated by MSs than macrocells. We assume our radio link is subjected to Rayleigh fading and log-normal shadowing. The composite distribution of the link gain  $G$  is

$$f_G(g) = \int_0^\infty \frac{1}{\Omega} e^{-g/\Omega} \frac{\alpha}{\sqrt{2\pi}\sigma_{\text{shadow}}\Omega} \times \exp\left(-\frac{(10 \log_{10} \Omega - \mu_\Omega)^2}{2\sigma_{\text{shadow}}^2}\right) \delta\Omega$$

$$\mu_\Omega = -\beta 10 \log_{10}(d) \quad (3)$$

where

$d$	distance between the MS and BS;
$\beta$	path loss exponent;
$\sigma_{\text{shadow}}$	shadow standard deviation;
$\alpha$	$= 10/\ln 10$ .

In [11], the composite Gamma-log-normal distribution is approximated by a simple log-normal distribution. For Rayleigh fading ( $m = 1$ ),  $G$ -distribution is characterized by the mean and variance of the approximate log-normal

$$E[G_{\text{[dB]}}] = -\beta 10 \log_{10}(d) - 2.50675$$

$$\text{Var}[G_{\text{[dB]}}] = \sigma_{\text{shadow}}^2 + 31.0254. \quad (4)$$

### A. Reverse Link

We first consider a simple single macrocell and microcell system to introduce our method of HMRC analysis. Then, we extend our analysis to a multicell system.

1) *Single Cell Model*: Consider a single microcell embedded within a macrocell as shown in Fig. 1. Using HMRC, the reverse CIR of MS  $i$  is

$$\text{CIR}_i = \text{CIR}_{\text{micro-}i} + \text{CIR}_{\text{macro-}i}$$

$$= \frac{C_{\text{micro-}i}}{I_{\text{micro-}i}} + \frac{C_{\text{macro-}i}}{I_{\text{macro-}i}} \quad (5)$$

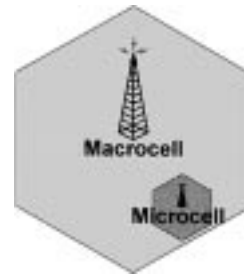


Fig. 1. Single cell model.

where  $C_{\text{micro-}i}$  and  $C_{\text{macro-}i}$  are the received signal power by the microcell BS and macrocell BS, respectively. Let  $\lambda_i$  be the ratio of the microcell interference to macrocell interference  $I_{\text{micro-}i}/I_{\text{macro-}i}$ . Then, the CIR <sub>$i$</sub>  becomes

$$\text{CIR}_i = \frac{C_{\text{micro-}i} + \lambda_i C_{\text{macro-}i}}{I_{\text{micro-}i}}$$

$$= \frac{(G_{\text{micro-}i} + \lambda_i G_{\text{macro-}i})P_i}{I_{\text{micro-}i}}$$

$$= \frac{C_{\text{reverse-}i}}{I_{\text{micro-}i}} \quad (6)$$

where  $G_{\text{micro-}i}$  and  $G_{\text{macro-}i}$  are the reverse-link gains associated with microcell and macrocell. HMRC reverse power control algorithm controls each MS transmit power  $P_i$  so that all MSs experience uniform CIR level. The convergence of such power control law has been proven in [12]. Let us assume that the microcell and macrocell both serve a large number of MSs, such that the microcell and macrocell interference levels experienced by each MS are nearly the same

$$I_{\text{micro-}i} \approx I_{\text{micro}}, \quad I_{\text{macro-}i} \approx I_{\text{macro}}, \quad \forall i. \quad (7)$$

Since the interference power is the difference between the total received power and the desired signal power, the differences in the desired signal components have minimal effect on interference values when the system load is relatively large. This also suggests that the variation in  $\lambda_i$  is minimal. The above assumption is justified numerically in Section III-A. Based on our assumption in (7), HMRC power control now results in all MSs having the same uniform combined signal power,  $C_{\text{reverse}}$ . Let  $N$  and  $M$  be the numbers of MSs located in microcell and macrocell, respectively, and express  $I_{\text{micro-}i}$  and  $I_{\text{macro-}i}$  as follows:

$$I_{\text{micro-}i} = \sum_{j \neq i}^N C_{\text{micro-}j}|_{\text{micro}} + \sum_{k=1}^M C_{\text{micro-}k}|_{\text{macro}}$$

$$I_{\text{macro-}i} = \sum_{j \neq i}^N C_{\text{macro-}j}|_{\text{micro}} + \sum_{k=1}^M C_{\text{macro-}k}|_{\text{macro}}$$

$i \in \text{Microcell}$

$$I_{\text{micro-}i} = \sum_{j=1}^N C_{\text{micro-}j}|_{\text{micro}} + \sum_{k \neq i}^M C_{\text{micro-}k}|_{\text{macro}}$$

$$I_{\text{macro-}i} = \sum_{j=1}^N C_{\text{macro-}j}|_{\text{micro}} + \sum_{k \neq i}^M C_{\text{macro-}k}|_{\text{macro}}$$

$i \in \text{Macrocell}$

$$(8)$$

where  $C_{cell1|cell2}$  is the received signal power by  $cell1$  given the MS is located in  $cell2$ . Let us first consider the case for the microcell MS. From (6), we can deduce that  $C_{macro-i} = (C_{reverse} - C_{micro-i})/\lambda_i$ . Therefore, see (9) shown at the bottom of the page. Solving the above equation for  $I_{micro-i}$  gives us

$$I_{micro-i} \approx \frac{(N + M - 1)C_{reverse}}{2}. \quad (10)$$

By using the similar approach, one can see that the macrocell MS yields the same result. Then, the reverse link CIR can be approximated as follows:

$$CIR_i = \frac{C_{reverse}}{I_{micro-i}} \approx \frac{2}{N + M - 1}. \quad (11)$$

We make some important observations about HMRC from (11). First, the CIR performance is independent of the microcell location. Without HMRC, the overall performance suffers from increased level of interlayer cross interference in cases where the microcell is closer to the macrocell BS. For HMRC, however, the combining effect is directly related to the proximity of the two BSs. Therefore, the increase in combining effect compensates for the increase in interference due to the microcell. Another worthy observation is that the HMRC performance is only limited by the overall system load  $N + M$  and not by individual cell loads. An overloaded microcell does not affect the system performance as long as the overall system load is kept under check, whereas it can dictate the system performance for non-HMRC systems. This suggests that HMRC is an effective way to share available resources between hierarchical layers.

2) *Multiple Cell Model:* We now extend our analysis to multiple-cell environments. Our multicell model consists of three macrocells and a cluster of  $K$  microcells embedded within the macrocells, as shown in Fig. 2. Then, as shown in (12) at the

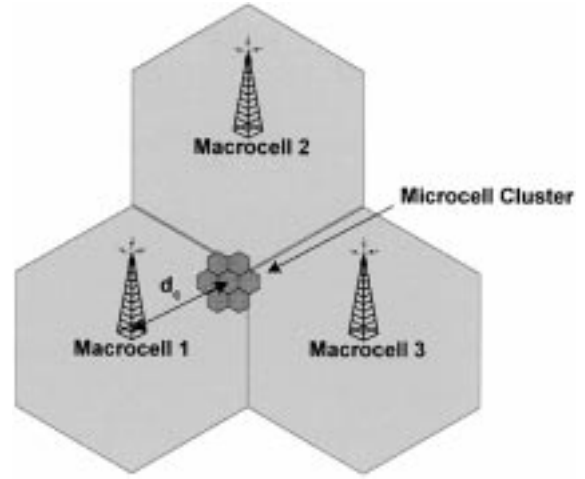


Fig. 2. Multiple cell model.

bottom of the next page,  $\lambda_{cell}$  is the ratio of  $I_{micro1}$  to  $I_{cell}$ . Let  $N_i$  and  $M_j$  be the numbers of MSs in microcell  $i$  and macrocell  $j$ , respectively. Then, for the microcell 1 MSs

$$\begin{aligned} I_{macro1-i} &= \sum_{j \neq i}^{N_1} C_{macro1-j|micro1} + \dots \\ &+ \sum_{l=1}^{N_K} C_{macro1-l|microK} \\ &+ \sum_{p=1}^{M_1} C_{macro1-p|macro1} + \dots \\ &+ \sum_{r=1}^{M_3} C_{macro1-r|macro3} \\ &\approx (N_1 + \dots + N_K + M_1 + M_2 + M_3 - 1) \\ &\times \frac{C_{reverse}}{\lambda_{macro1-i}} - (2 + K) \frac{I_{micro1-i}}{\lambda_{macro1-i}}. \end{aligned}$$

$$\begin{aligned} \lambda_i &= \frac{I_{micro-i}}{I_{macro-i}} \\ &= \frac{I_{micro-i}}{\sum_{j \neq i}^N C_{macro-j|micro} + \sum_{k=1}^M C_{macro-k|macro}} \\ &= \frac{I_{micro-i}}{\sum_{j \neq i}^N (C_{reverse} - C_{micro-j|micro})/\lambda_j + \sum_{k=1}^M (C_{reverse} - C_{micro-k|macro})/\lambda_k} \\ &\approx \frac{\lambda_i I_{micro-i}}{\sum_{j \neq i}^N (C_{reverse} - C_{micro-j|micro}) + \sum_{k=1}^M (C_{reverse} - C_{micro-k|macro})}, \quad \lambda_j \approx \lambda_k \quad \forall j, k \\ &\approx \frac{\lambda_i I_{micro-i}}{(N + M - 1)C_{reverse} - I_{micro-i}} \end{aligned} \quad (9)$$

Therefore

$$I_{\text{micro}1-i} \approx \frac{(N_1 + \dots + N_K + M_1 + M_2 + M_3 - 1)C_{\text{reverse}}}{3 + K}$$

$$\text{CIR}_i \approx \frac{3 + K}{N_1 + \dots + N_K + M_1 + M_2 + M_3 - 1}. \quad (13)$$

Using MSs in other cells and  $\lambda_s$  gives us the same result. We can make the same important observations we made in the single-cell case for multicell case also. Note also that by assuming both microcells and macrocells are loaded with an equal number of MSs, our result obtained in (13) is the same result obtained in [5]. This tells us that the macrocell capacity is nearly unaffected by introducing microcell(s) when interlayer HMRC is allowed.

### B. Forward Link

We use a single-cell hierarchical model as in Fig. 1 for our forward analysis. One should be able to easily extend the given result to multicell environments. Our forward analysis consists of two parts: non-STD and STD cases. For a non-STD case, there is no transmit diversity; each BS has only one antenna and provides single forward transmit path. Each MS connects to the BS, which provides the most robust path. The formulation of our analysis is partly based on the framework outlined in [13].

1) *Non-STD*: Given the location of an MS  $r$  and  $\theta$ , the forward transmit power according to NNP is

$$P_{\text{micro}i}(r, \theta) = \frac{(1/\gamma)G_{\text{macro}i} + G_{\text{micro}i}}{G_{\text{micro}i}} P_T$$

$$= \left( \frac{G_{\text{macro}i}}{\gamma G_{\text{micro}i}} + 1 \right) P_T$$

$$= \left( \frac{1}{\gamma} 10^{(\xi_{\text{macro}}(r, \theta) - \xi_{\text{micro}}(r, \theta))/10} + 1 \right) P_T$$

$$= \left( \frac{1}{\gamma} 10^{x(r, \theta)/10} + 1 \right) P_T,$$

if  $G_{\text{micro}i} > G_{\text{macro}i}$

$$P_{\text{macro}j}(r, \theta) = \frac{(1/\gamma)G_{\text{macro}j} + G_{\text{micro}j}}{G_{\text{macro}j}} P_T$$

$$= \left( \frac{1}{\gamma} + 10^{(\xi_{\text{micro}}(r, \theta) - \xi_{\text{macro}}(r, \theta))/10} \right) P_T$$

$$= \left( \frac{1}{\gamma} + 10^{y(r, \theta)/10} \right) P_T$$

if  $G_{\text{micro}j} < G_{\text{macro}j}$ . (14)

Let us now compute the conditional cumulative-distribution functions (cdfs) of  $Z = 10^{x(r, \theta)/10}$  and  $W = 10^{y(r, \theta)/10}$ .

$$F_Z(z|r, \theta) = \frac{P[10^{x(r, \theta)/10} < z|r, \theta]}{P[10^{x(r, \theta)/10} < 1|r, \theta]}$$

$$= \frac{P[x(r, \theta) < 10 \log_{10}(z)|r, \theta]}{P[x(r, \theta) < 0|r, \theta]}$$

$$= \Phi \left[ \frac{10 \log_{10}(z) - \mu_x(r, \theta)}{\sigma_x} \right] / \Phi \left[ \frac{-\mu_x(r, \theta)}{\sigma_x} \right]$$

$0 < z < 1$

$$F_W(w|r, \theta) = \Phi \left[ \frac{10 \log_{10}(w) - \mu_y(r, \theta)}{\sigma_y} \right] / \Phi \left[ \frac{-\mu_y(r, \theta)}{\sigma_y} \right]$$

$0 < w < 1$  (15)

where

$$\mu_x(r, \theta) = \mu_{\xi_{\text{macro}}}(r, \theta) - \mu_{\xi_{\text{micro}}}(r, \theta)$$

$$= -\beta 10 \log_{10}[d_{\text{macro}}(r, \theta)]$$

$$+ \beta 10 \log_{10}[d_{\text{micro}}(r, \theta)]$$

$$\mu_y(r, \theta) = \mu_{\xi_{\text{micro}}}(r, \theta) - \mu_{\xi_{\text{macro}}}(r, \theta)$$

$$\sigma_x^2 = \sigma_y^2 = 2(\sigma_{\text{shadow}}^2 + 31.0254). \quad (16)$$

Then, the cdfs of  $Z$  and  $W$  are

$$F_Z(z) = \int_0^{2\pi} \frac{\delta\theta}{2\pi} \int_0^{R_{\text{micro}}} \frac{2r\delta r}{R_{\text{micro}}^2} F_Z(z|r, \theta)$$

if MS  $\in$  Microcell

$$F_W(w) = \int_0^{2\pi} \frac{\delta\theta}{2\pi} \int_0^{R_{\text{macro}}} \frac{2r\delta r}{R_{\text{macro}}^2} F_W(w|r, \theta)$$

if MS  $\in$  Macrocell. (17)

Since both  $Z$  and  $W$  are non-negative random variables, their expected values are given as follows:

$$E[Z] = \int_0^\infty [1 - F_Z(z)] \delta z$$

$$= \int_0^1 [1 - F_Z(z)] \delta z$$

$$E[W] = \int_0^1 [1 - F_W(w)] \delta w. \quad (18)$$

Let  $N$  and  $M$  be the numbers of MSs in microcell and macrocell, respectively. Assuming there are  $N'$  microcell MS con-

$$\text{CIR}_i = \text{CIR}_{\text{micro}1-i} + \dots + \text{CIR}_{\text{micro}K-i} + \text{CIR}_{\text{macro}1-i} + \dots + \text{CIR}_{\text{macro}3-i}$$

$$= \frac{C_{\text{micro}1-i} + \dots + \lambda_{\text{micro}K-i} C_{\text{micro}K-i} + \lambda_{\text{macro}1-i} C_{\text{macro}1-i} + \dots + \lambda_{\text{macro}3-i} C_{\text{macro}3-i}}{I_{\text{micro}1-i}}$$

$$= \frac{C_{\text{reverse}i}}{I_{\text{micro}1-i}} \quad (12)$$

nected to microcell and  $M'$  macrocell MSs connected to macrocell, the expected value of the total forward transmit power by each BS is

$$\begin{aligned}
& E[P_{\text{micro}}|N', M'] \\
&= N' P_T \left( \frac{E[Z|\text{Microcell}]}{\gamma} + 1 \right) \\
&+ (M - M') P_T \left( \frac{E[Z|\text{Macrocell}]}{\gamma} + 1 \right) \\
& E[P_{\text{macro}}|N', M'] \\
&= (N - N') P_T \left( \frac{1}{\gamma} + E[W|\text{Microcell}] \right) \\
&+ M' P_T \left( \frac{1}{\gamma} + E[W|\text{Macrocell}] \right). \quad (19)
\end{aligned}$$

We know that  $N'$  and  $M'$  are binomial random variables with probabilities  $\text{Pr}_{\text{micro}}$  and  $\text{Pr}_{\text{macro}}$ , respectively. Then

$$\begin{aligned}
E[P_{\text{micro}}] &= \sum_{N'=0}^N \binom{N}{N'} \text{Pr}_{\text{micro}}^{N'} (1 - \text{Pr}_{\text{micro}})^{N-N'} \\
&\times \sum_{M'=0}^M \binom{M}{M'} \text{Pr}_{\text{macro}}^{M'} (1 - \text{Pr}_{\text{macro}})^{M-M'} \\
&\times E[P_{\text{micro}}|N', M'] \\
E[P_{\text{macro}}] &= \sum_{N'=0}^N \binom{N}{N'} \text{Pr}_{\text{micro}}^{N'} (1 - \text{Pr}_{\text{micro}})^{N-N'} \\
&\times \sum_{M'=0}^M \binom{M}{M'} \text{Pr}_{\text{macro}}^{M'} (1 - \text{Pr}_{\text{macro}})^{M-M'} \\
&\times E[P_{\text{macro}}|N', M'] \quad (20)
\end{aligned}$$

where

$$\begin{aligned}
\text{Pr}_{\text{micro}} &= P[G_{\text{micro-}i} > G_{\text{macro-}i} | i \in \text{Microcell}] \\
&= 1 - \int_0^{2\pi} \frac{\delta\theta}{2\pi} \int_0^{R_{\text{micro}}} \frac{2r\delta r}{R_{\text{micro}}^2} \Phi \\
&\times \left( \frac{\mu_{\text{macro}}(r, \theta) - \mu_{\text{micro}}(r, \theta)}{\sqrt{2(\sigma_{\text{shadow}}^2 + 31.0254)}} \right) \\
\text{Pr}_{\text{macro}} &= P[G_{\text{macro-}j} > G_{\text{micro-}j} | j \in \text{Macrocell}] \\
&= \int_0^{2\pi} \frac{\delta\theta}{2\pi} \int_0^{R_{\text{macro}}} \frac{2r\delta r}{R_{\text{macro}}^2} \Phi \\
&\times \left( \frac{\mu_{\text{macro}}(r, \theta) - \mu_{\text{micro}}(r, \theta)}{\sqrt{2(\sigma_{\text{shadow}}^2 + 31.0254)}} \right). \quad (21)
\end{aligned}$$

We let  $\gamma = E[P_{\text{micro}}]/E[P_{\text{macro}}]$  and run iterations until  $\gamma$  converges. Then, the forward CIR is

$$\text{CIR}_{\text{non-STD}} = \frac{P_T}{P_{\text{micro}}} \approx \frac{P_T}{E[P_{\text{micro}}]}. \quad (22)$$

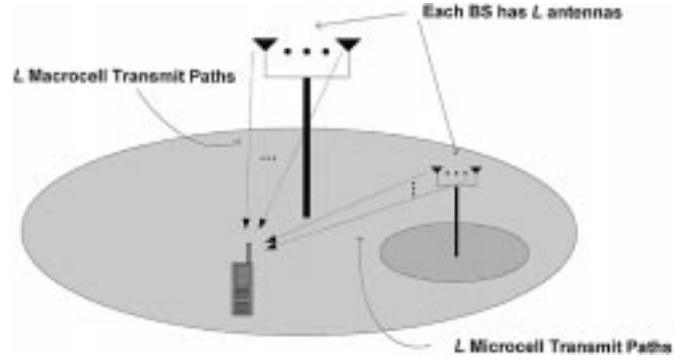


Fig. 3. Selective transmit diversity.

2) *STD*: In STD, each BS has a number of spatially separated antennas and the orthogonal pilot signal is transmitted from each antenna, as shown in Fig. 3. In order for the fading conditions associated with different antennas to be sufficiently uncorrelated from one another (less than 0.7 correlation), the antenna separation needs to be on the order of ten wavelengths apart [14]. By way of monitoring the pilot signals, an MS can select (mobile-assisted) the antenna that provides the most robust forward transmit path and have it transmit the signal until a better antenna is found. Therefore, only one antenna is selected to transmit at a time with STD, but the selected antenna provides the best signal path among multiple antennas. The main difference between STD and non-STD schemes is that STD provides multiple potential transmit paths per BS with uncorrelated fading, while non-STD provides one path per BS. However, both STD and non-STD allows only one antenna to transmit at a time. Diversity gain through antenna separation is viable at BS sites where the space and system complexity are less of limiting factors. We assume the antennas are separated sufficiently far apart that all potential transmit paths from the same BS have uncorrelated fading but correlated shadowing.

Let us now assume that both microcell and macrocell BSs have  $L$  antennas each, which means that the MS selects the best antenna out of potential  $2L$  antennas. Let  $P_{\text{cell}}^{(l)}$  be the total forward transmit power by the  $l$ th transmit branch of *cell*. Since the MSs are uniformly distributed, each transmit branch within a cell has an equal probability of being selected by the MSs, and, therefore, we can assume that

$$\begin{aligned}
P_{\text{micro}}^{(i)} &\approx P_{\text{micro}}^{(j)} \approx P_{\text{micro}}^{\text{STD}} \\
P_{\text{macro}}^{(i)} &\approx P_{\text{macro}}^{(j)} \approx P_{\text{macro}}^{\text{STD}}, \quad i \neq j. \quad (23)
\end{aligned}$$

Then, the forward transmit power for MS  $i$  is shown in (24) at the bottom of the next page, where  $\gamma_{\text{STD}} = P_{\text{micro}}^{\text{STD}}/P_{\text{macro}}^{\text{STD}}$  and  $G_{\text{cell}}^{(l)}$  is the forward gain associated with  $l$ th transmit branch of *cell*. Let  $G_{\text{cell-}i} = \max[G_{\text{cell-}i}^{(1)}, \dots, G_{\text{cell-}i}^{(L)}]$ ; then, the cdf of  $G_{\text{cell-}i}^{(l)}/G_{\text{cell-}i}$  is

$$\begin{aligned}
P \left[ G_{\text{cell-}i}^{(l)}/G_{\text{cell-}i} < x \right] &= \frac{P \left[ G_{\text{cell-}i}^{(l)}/G_{\text{cell-}i} < x \right]}{P \left[ G_{\text{cell-}i}^{(l)}/G_{\text{cell-}i} < 1 \right]} \\
&\approx \frac{2x}{x+1}, \quad 0 < x < 1 \quad (25)
\end{aligned}$$

where  $P[G_{\text{cell-}i}^{(l)}/G_{\text{cell-}i} < x] = x/(x+1)$ . The above result is accurate for  $L = 2$  and adequate for  $L = 3$  since the greatest

diversity gain occurs between  $L = 1$  and  $L = 2$  [11]. For two different cell locations, we can assume  $G_{\text{cell}_k-i}^{(l)}$  and  $G_{\text{cell}_j-i}$  are independent. Because the transmit paths from the same BS experience independent Rayleigh fading and correlated shadowing, the conditional pdf and pdf of  $G_{\text{cell}_i}$  are

$$f_{G_{\text{cell}_i}}(g|\Omega) = \frac{L}{\Omega} e^{-g/\Omega} (1 - e^{-g/\Omega})^{L-1}$$

$$f_{G_{\text{cell}_i}}(g) = \int_0^\infty f_{G_{\text{cell}_i}}(g|\Omega) \frac{\alpha}{\sqrt{2\pi}\sigma_{\text{shadow}}\Omega} \times \exp\left(-\frac{(10 \log_{10} \Omega - \mu_\Omega)^2}{2\sigma_{\text{shadow}}^2}\right) \delta\Omega. \quad (26)$$

It is shown in [11] that  $f_{G_{\text{cell}_i}}(g)$  can be approximated by a purely log-normal distribution for  $L = 2$  with mean and variance given by

$$\mu_G = \alpha[\ln 2 - C] + \mu_\Omega = 0.503552 - \beta \log_{10}(d)$$

$$\sigma_G^2 = \alpha^2[\zeta(2, 1) - 2(\ln 2)^2] + \sigma_{\text{shadow}}^2 = 12.9016 + \sigma_{\text{shadow}}^2 \quad (27)$$

where  $C \simeq 0.5772$  is Euler's constant, and  $\zeta(2, 1) = \sum_{k=0}^\infty 1/(1+k)^2$  is Reimann's zeta function. Appendix B derives a similar approximation for  $L = 3$ , and we obtain the following mean and variance:

$$\mu_G = \alpha[3 \ln 2 - \ln 3 - C] + \mu_\Omega = 1.75294 - \beta \log_{10}(d)$$

$$\sigma_G^2 = \alpha^2[\zeta(2, 1) - 12(\ln 2)^2 + 6 \ln 2 \ln 3] + \sigma_{\text{shadow}}^2 = 8.4592 + \sigma_{\text{shadow}}^2. \quad (28)$$

Then, the conditional cdf and cdf of  $G_{\text{cell}_k-i}^{(l)}/G_{\text{cell}_j-i}$  are

$$P\left[G_{\text{cell}_k-i}^{(l)}/G_{\text{cell}_j-i} < x|r, \theta\right]$$

$$= \frac{P\left[G_{\text{cell}_k-i}^{(l)}/G_{\text{cell}_j-i} < x|r, \theta\right]}{P\left[G_{\text{cell}_k-i}^{(l)}/G_{\text{cell}_j-i} < 1|r, \theta\right]}$$

$$= \Phi\left[\frac{10 \log_{10}(x) - \mu_{kj}(r, \theta)}{\sigma_{kj}}\right] / \Phi\left[\frac{-\mu_{kj}(r, \theta)}{\sigma_{kj}}\right]$$

$$P\left[G_{\text{cell}_k-i}^{(l)}/G_{\text{cell}_j-i} < x\right]$$

$$= \int_0^{2\pi} \frac{\delta\theta}{2\pi} \int_0^{R_{\text{cell}}} \frac{2r\delta r}{R_{\text{cell}}^2} P\left[G_{\text{cell}_k-i}^{(l)}/G_{\text{cell}_j-i} < x|r, \theta\right]$$

$$0 < x < 1 \quad (29)$$

where

$$\mu_{kj}(r, \theta) = \mu_{\xi_{\text{cell}_k}}(r, \theta) - \mu_{G_{\text{cell}_j}}(r, \theta)$$

$$= -\beta 10 \log_{10}[d_{\text{cell}_k}(r, \theta)] - 2.50675$$

$$+ \mu_{G_{\text{cell}_j}}(r, \theta)$$

$$\sigma_{kj}^2 = \sigma_{\text{cell}_k}^2 + \sigma_G^2$$

$$= \sigma_{\text{shadow}}^2 + 31.0254 + \sigma_G^2. \quad (30)$$

We can derive the expected values of  $P_{\text{micro-}i}^{\text{STD}}$  and  $P_{\text{macro-}i}^{\text{STD}}$  using the same approach used in the previous section and get

$$E[P_{\text{micro-}i}^{\text{STD}}] = \left(\frac{L}{\gamma_{\text{STD}}} E[Z] + (L-1)E[X] + 1\right) P_T$$

$$E[P_{\text{macro-}i}^{\text{STD}}] = \left(\frac{L-1}{\gamma_{\text{STD}}} E[Y] + LE[W] + \frac{1}{\gamma_{\text{STD}}}\right) P_T \quad (31)$$

where

$$Z = G_{\text{macro-}i}^{(l)}/G_{\text{micro-}i}$$

$$X = G_{\text{micro-}i}^{(l)}/G_{\text{micro-}i}$$

$$Y = G_{\text{macro-}i}^{(l)}/G_{\text{macro-}i}$$

$$W = G_{\text{micro-}i}^{(l)}/G_{\text{macro-}i}, \quad 0 < Z, X, Y, W < 1. \quad (32)$$

Since each transmit branch has equal chance of being selected, the expected value of the total forward transmit power by each BS branch, given  $N'$  and  $M'$ , is

$$E[P_{\text{micro}}^{\text{STD}}|N', M'] = \frac{N'}{L} P_T E[P_{\text{micro-}i}^{\text{STD}}|\text{Microcell}]$$

$$+ \frac{M-M'}{L} P_T E[P_{\text{micro-}i}^{\text{STD}}|\text{Macrocell}]$$

$$E[P_{\text{macro}}^{\text{STD}}|N', M'] = \frac{N-N'}{L} P_T E[P_{\text{macro-}i}^{\text{STD}}|\text{Microcell}]$$

$$+ \frac{M'}{L} P_T E[P_{\text{macro-}i}^{\text{STD}}|\text{Macrocell}]. \quad (33)$$

$E[P_{\text{micro}}^{\text{STD}}]$  and  $E[P_{\text{macro}}^{\text{STD}}]$  can now be computed as in (20) with the following  $\Pr_{\text{micro}}$  and  $\Pr_{\text{macro}}$ :

$$\Pr_{\text{micro}} = P\left[\max\left[G_{\text{micro-}i}^{(1)}, \dots, G_{\text{micro-}i}^{(L)}\right] > \max\right.$$

$$\left.\times \left[G_{\text{macro-}i}^{(1)}, \dots, G_{\text{macro-}i}^{(L)}\right] | i \in \text{Microcell}\right]$$

$$= P[G_{\text{micro-}i} > G_{\text{macro-}i} | i \in \text{Microcell}]$$

$$\Pr_{\text{macro}} = P[G_{\text{macro-}i} > G_{\text{micro-}i} | i \in \text{Macrocell}] \quad (34)$$

$$P_{\text{micro-}i}^{\text{STD}}(r, \theta) = \frac{(1/\gamma_{\text{STD}}) \left(G_{\text{macro-}i}^{(1)} + \dots + G_{\text{macro-}i}^{(L)}\right) + G_{\text{micro-}i}^{(1)} + \dots + G_{\text{micro-}i}^{(L)}}{\max\left[G_{\text{micro-}i}^{(1)}, \dots, G_{\text{micro-}i}^{(L)}\right]} P_T$$

$$\text{if } \max\left[G_{\text{micro-}i}^{(1)}, \dots, G_{\text{micro-}i}^{(L)}\right] > \max\left[G_{\text{macro-}i}^{(1)}, \dots, G_{\text{macro-}i}^{(L)}\right]$$

$$P_{\text{macro-}i}^{\text{STD}}(r, \theta) = \frac{(1/\gamma_{\text{STD}}) \left(G_{\text{macro-}i}^{(1)} + \dots + G_{\text{macro-}i}^{(L)}\right) + G_{\text{micro-}i}^{(1)} + \dots + G_{\text{micro-}i}^{(L)}}{\max\left[G_{\text{macro-}i}^{(1)}, \dots, G_{\text{macro-}i}^{(L)}\right]} P_T$$

$$\text{if } \max\left[G_{\text{micro-}i}^{(1)}, \dots, G_{\text{micro-}i}^{(L)}\right] < \max\left[G_{\text{macro-}i}^{(1)}, \dots, G_{\text{macro-}i}^{(L)}\right]. \quad (24)$$

TABLE I  
SINGLE CELL MODEL REVERSE PERFORMANCE RESULTS

$N$	$M$	$CIR_{analytical}$	$CIR_{simulation}$
10	10	-9.60 dB	-9.78 dB
15	10	-10.66 dB	-10.79 dB
20	15	-12.21 dB	-12.30 dB
20	20	-12.82 dB	-12.90 dB

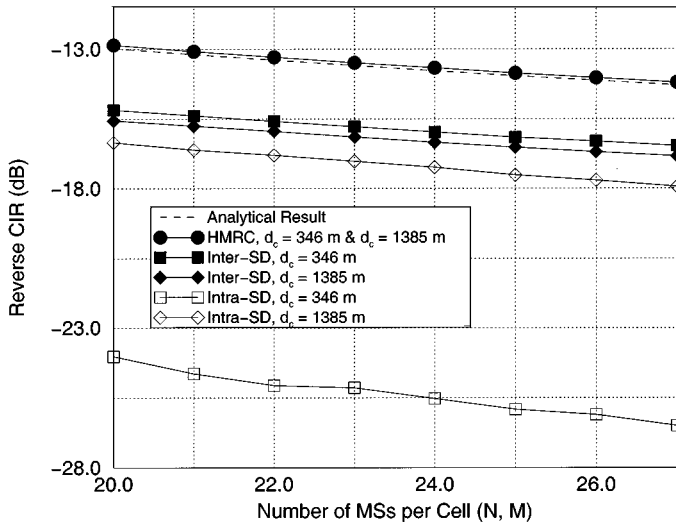


Fig. 4. Reverse-link CIR performance comparison.

### III. NUMERICAL RESULTS

A path loss exponent of 4 and a shadow standard deviation of 8 dB are used in the simulation. The radii of the macrocell and microcell regions are set to 1500 and 200 m, respectively.

#### A. Reverse Link

Table I shows the average CIR performance comparison between our analytical and simulation results obtained using the single-cell model. Our analytical results closely match the simulation results. Small deviations between the two results are most likely caused by our equal interference assumption in (7) while deriving the analytical solution. The fact is that MSs located close to a BS experience less interference, while MSs further away from the BS face higher interference. However, the difference is very marginal, it becomes even smaller as the system load increases, and our assumption becomes a better representation of the system with higher loads.

Fig. 4 shows the multicell reverse-link CIR performance comparison between HMRC and non-HMRC diversity power control schemes at various microcell cluster locations ( $d_c$ ). A three-macrocell and three-microcell model is used to obtain the simulation results. Both macrocells and microcells are loaded with the same number of MSs. Two non-HMRC diversity schemes are compared: intralayer selection diversity (intra-SD) and interlayer selection diversity (inter-SD). With intra-SD the most robust link within each layer is selected, while inter-SD allows each MS to connect the best BS at any layer. Clearly, HMRC performance is superior to that of non-HMRC

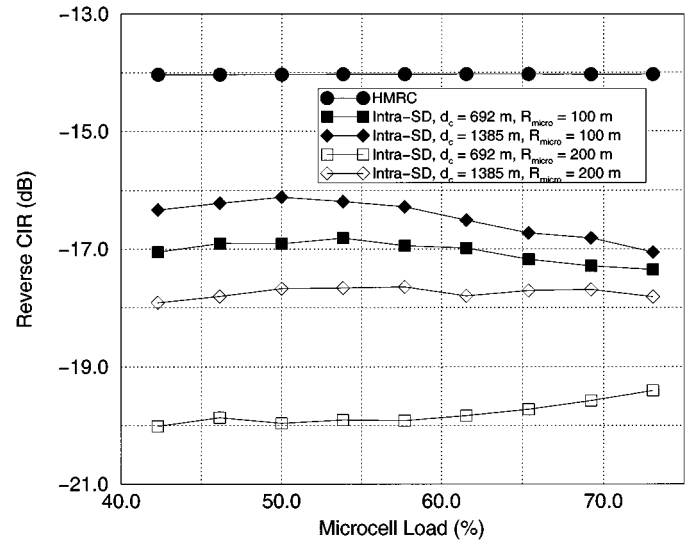


Fig. 5. Intra-SD CIR performance versus microcell load.

schemes. It is observed that both macrocell and microcell capacities are nearly unaffected by each other's presence (i.e., both macrocells and microcells retain a near-isolated cell capacity). The performances of both SD schemes are dependent of the microcell cluster location  $d_c$ . For intra-SD, the cross interference between the layers increases as the microcell cluster gets closer to a macrocell BS and causes overall system performance degradation. For inter-SD, the diversity gain decreases as  $d_c$  increases, which also causes the performance to suffer. However, employing HMRC eliminates the effect of the cluster location on the CIR performance. From (12), one can see that the reverse CIR performance of HMRC is proportional to the  $\lambda_i$  and macrocell gains. These two factors balance the performance as the microcell cluster location changes. When  $d_c$  is small, the cross interference causes the  $\lambda_i$  to decrease, but the loss is compensated by the increase in macrocell gains. Conversely, when  $d_c$  is large, the macrocell gains decrease while the  $\lambda_i$  increase.

Our analytical results indicate that the HMRC performance is a function of the overall system load and does not depend on either the load distribution between the layers or the cell sizes. Figs. 5 and 6 show the effect of microcell load and size on the reverse-link CIR performance. The same three-multicell model is used in this simulation also. The overall system load is kept at 156 MSs, while the microcell load percentage to the overall load is varied. It is observed that in nearly all instances both non-HMRC schemes suffer performance losses with an increase in the microcell load percentage and microcell radius  $R_{micro}$ . It can be understood that the increase in the overall interference due to an increased microcell load cannot be relieved entirely by a decreased macrocell load. Larger microcell sizes also increase interference, since MSs belong to microcells need to transmit at higher power levels. The performance of HMRC is not affected by the microcell load and size changes, as predicted. The increase in microcell interference also increases the  $\lambda_i$ , which offsets the negative effect of the microcell interference. Therefore, HMRC allows flexible resource sharing between hierarchical layers.

TABLE II  
SINGLE CELL MODEL FORWARD PERFORMANCE RESULTS

N	M	Non-STD		STD, L = 2		STD, L = 3	
		CIR <sub>analytical</sub>	CIR <sub>simulation</sub>	CIR <sub>analytical</sub>	CIR <sub>simulation</sub>	CIR <sub>analytical</sub>	CIR <sub>simulation</sub>
10	10	-11.54 dB	-11.21 dB	-9.99 dB	-9.65 dB	-9.31 dB	-8.86 dB
15	10	-12.80 dB	-12.56 dB	-11.25 dB	-11.02 dB	-10.57 dB	-10.20 dB
20	15	-14.19 dB	-14.02 dB	-12.64 dB	-12.46 dB	-11.96 dB	-11.67 dB
20	20	-14.56 dB	-14.40 dB	-13.01 dB	-12.84 dB	-12.34 dB	-12.04 dB

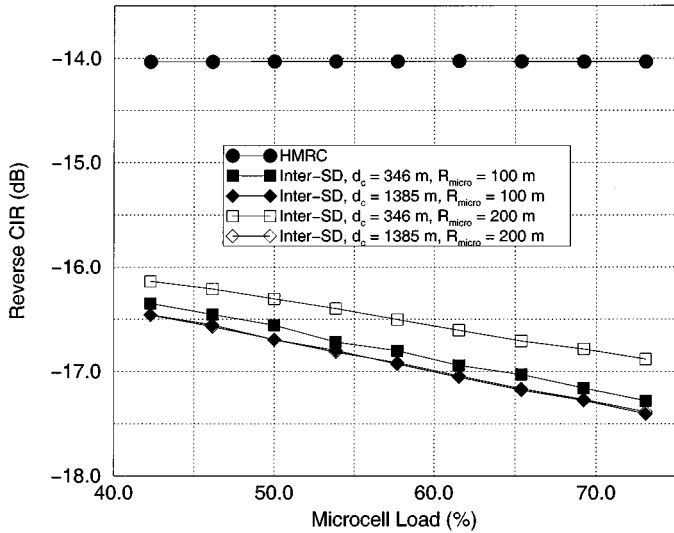


Fig. 6. Inter-SD CIR performance versus microcell load.

Our observations suggest that implementing HMRC gives system planners and administrators almost unlimited freedom and flexibility when contemplating microcell placements. With HMRC, microcell(s) can be placed anywhere within the existing macrocell layer, significant performance and capacity gains can be obtained while guaranteeing robust resource sharing between the layers.

B. Forward Link

Our forward analytical results are computed using *Mathematica*, and less than 15 iteration loops are needed to get the convergence in the  $\gamma$ s. Table II compares the analytical and simulation results of the single-cell model. These results are obtained with  $d_c = 692$  m. Both results are in good agreement with each other, while the analytical results exhibit lower values than the simulation results. This is due to our analytical interference assumption in (A.1), which results in a pessimistic interference level. However, the differences become marginal as the number of MSs increases. Table II also shows the results obtained with STD. Again, we observe that our analytical results closely follow the simulation results. One can immediately see the benefit of employing STD on forward performance. With two-branch transmit diversity, the forward CIR performance improves by 1.5 dB and 2.5 dB with three-branch transmit diversity. Fig. 7 compares the analytical and simulation forward performance results as a function of the microcell location  $d_c$ , while

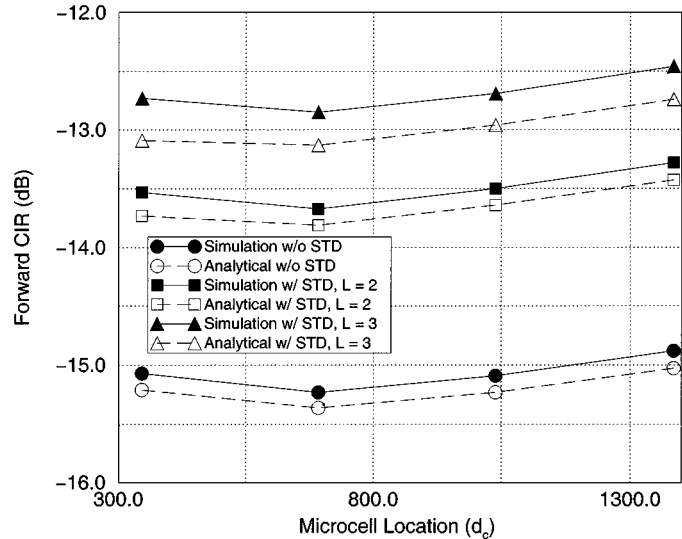


Fig. 7. Forward performance versus microcell location.

the system load is fixed at 24 MSs per cell. Again, we observe that our analytical model does an excellent job of predicting the simulation results. We notice that the differences between the analytical and simulation results in the figure are larger for  $L = 3$  than  $L = 2$  due to our assumption in (25). But, the differences are still small considering they are within 0.3 dB.

Fig. 8 shows the average forward performance results obtained from our multicell model, which consists of three macrocells and a cluster of three microcells. The benefit of STD is also evident from these results where the system benefits from the added diversity effect due to multiple cell locations. Although the performance varies slightly, both non-STD and STD effectively neutralize the effect of the microcell cluster location on forward performance. One interesting observation is that forward performance improves slightly as  $d_c$  decreases. Although the forward cross interference between the layers increases with smaller  $d_c$ , the system takes advantage of increased interlayer diversity effect, which ultimately results in improved performance.

Fig. 9 shows the effect of the microcell cluster size on the forward performance. The plot shows the performance comparison between single-cell cluster and three-cell cluster. We have observed in the previous section that HMRC allows microcell(s) to be added without impacting the existing reverse-link capacity. With STD, however, the forward performance does depend on the microcell cluster size and that an increase in the number of microcells in the cluster causes the performance to suffer. The

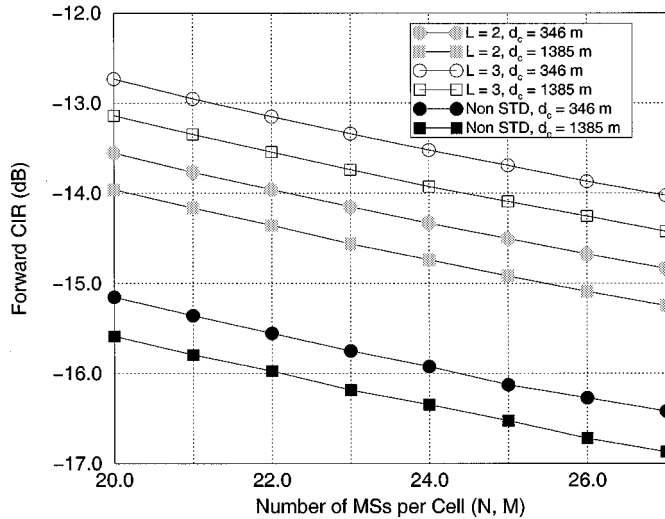


Fig. 8. Forward performance in multicell model.

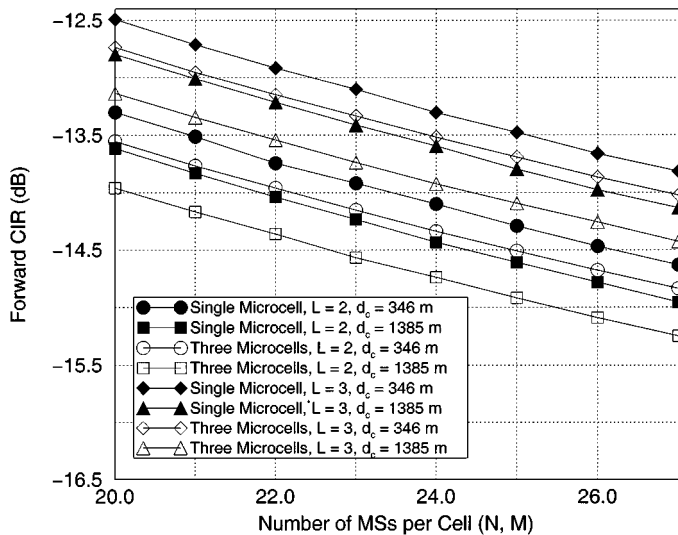


Fig. 9. Forward performance versus microcell cluster size.

added diversity effect is apparently not enough to fully compensate for increase in interference resulting from the microcell increase. Yet, the performance degradation is negligible considering the capacity gain obtained by adding microcell(s). For example, assuming the target CIR is set to  $-14$  dB, a three-macrocell system with a single-cell cluster has capacity of 26 MSs per cell at  $d_c = 1385$  m with  $L = 3$ . With the same exact setting, the same system with three-cell cluster achieves 24 MSs per cell, yet its overall system capacity is far greater due to the added microcells.

In Figs. 4 and 8, we observe that a forward link performance comparable to the reverse HMRC performance can be achieved by implementing STD with  $L = 3$ . Not only does STD improve the forward performance, but it can also benefit the reverse link performance by providing additional BS antenna elements for stronger combining.

#### IV. CONCLUSION

We have implemented HMRC and STD in CDMA hierarchical systems in order to study their effectiveness and feasibility. We have derived simple analytical solutions for reverse-link HMRC and forward-link STD CIR performance, and these solutions are verified by an extensive simulation study. Our results indicate that a hierarchical system approach is indeed a viable solution for increasing CDMA reverse link capacity-performance when macrodiversity schemes are implemented. It is shown that a higher system capacity can be achieved without assigning disjoint spectrum between hierarchical layers by utilizing HMRC and STD.

There is a number of significant implementation issues that need to be addressed in order to realize HMRC and STD. Both HMRC and HNNP are essentially centralized power control schemes which require central control stations to perform all the important control functions for the entire system. For HMRC, combining signals from several BSs requires fast and reliable links among BSs and adds a considerable overhead to the system, since every MS is in soft handoff mode with surrounding BSs all the time. STD needs each BS to transmit  $L$  separate pilot signals and a mechanism to select a particular path out of all the available ones [8]. No formal standard using HMRC has been proposed yet, but a possible implementation can take a form of distributed antenna systems [15] with optical fiber links among the antennas [16]. Transmit diversity schemes, such as orthogonal transmission diversity (OTD), time switched transmission diversity (TSTD), and STD, have already been proposed in major IMT-2000 standards, and it has been verified in [8] and [17] that STD provides better performance than OTD and TSTD. Our main purpose for the study is to investigate the means of achieving high capacity/performance hierarchical CDMA systems which share the same spectrum between layers, and we have shown that such systems are indeed possible.

#### APPENDIX A HIERARCHICAL NNP

Let us assume that there are  $K$  microcells surrounded by three macrocells as in Fig. 2. Let  $P_{macroj}$  and  $P_{microk}$  be the total powers transmitted by macrocell  $j$  and microcell  $k$ , respectively. Then, the interference experienced by MS  $i$  can be estimated as

$$I_i \approx G_{macro1-i} P_{macro1} + \dots + G_{macro3-i} P_{macro3} + G_{micro1-i} P_{micro1} + \dots + G_{microK-i} P_{microK}. \quad (A.1)$$

Let  $\gamma_{cell}$  be the ratio between  $P_{micro1}$  and  $P_{cell}$ . Only one BS can transmit to MS  $i$  at a given instant and the transmit power is determined by (A.2), shown at the top of the next page when MS  $i$  is connected to BS  $cell$  and  $P_T$  is the predetermined forward transmit power constant. The resulting forward CIR is then shown in (A.3) at the top of the next page. Notice that with NNP, every MS experiences the same forward CIR level, regardless of its location.

$$P_{cell_i} = \frac{\frac{1}{\gamma_{macro1}} G_{macro1_i} + \cdots + \frac{1}{\gamma_{macro3}} G_{macro3_i} + G_{micro1_i} + \cdots + \frac{1}{\gamma_{microK}} G_{microK_i}}{G_{cell_i}} P_T \quad (A.2)$$

$$\begin{aligned} CIR_i &= \frac{C_i}{I_i} \\ &\approx \frac{\left( \frac{1}{\gamma_{macro1}} G_{macro1_i} + \cdots + \frac{1}{\gamma_{macro3}} G_{macro3_i} + G_{micro1_i} + \cdots + \frac{1}{\gamma_{microK}} G_{microK_i} \right) P_T}{\left( \frac{1}{\gamma_{macro1}} G_{macro1_i} + \cdots + \frac{1}{\gamma_{macro3}} G_{macro3_i} + G_{micro1_i} + \cdots + \frac{1}{\gamma_{microK}} G_{microK_i} \right) P_{micro1}} \\ &\approx \frac{P_T}{P_{micro1}} \end{aligned} \quad (A.3)$$

#### APPENDIX B DERIVATION OF (28)

For  $L = 3$ , the mean of log-normal approximation is

$$\begin{aligned} E[10 \log_{10} g] &= \int_0^\infty \int_0^\infty 10 \log_{10} g \frac{3}{\Omega} e^{-g/\Omega} (1 - e^{-g/\Omega})^2 \\ &\quad \times \frac{\alpha}{\sqrt{2\pi}\sigma_{shadow}\Omega} \exp\left(-\frac{(10 \log_{10} \Omega - \mu_\Omega)^2}{2\sigma_{shadow}^2}\right) \delta g \delta \Omega \\ &= \frac{\alpha}{\Omega} \int_0^\infty \frac{\alpha}{\sqrt{2\pi}\sigma_{shadow}\Omega} \exp\left(-\frac{(10 \log_{10} \Omega - \mu_\Omega)^2}{2\sigma_{shadow}^2}\right) \\ &\quad \times \int_0^\infty 3 \ln g (e^{-x/\Omega} - 2e^{-2x/\Omega} + e^{-3/\Omega}) \delta g \delta \Omega. \quad (B.4) \end{aligned}$$

According to [18, (4.352.1)]

$$\begin{aligned} &\int_0^\infty 3 \ln g (e^{-x/\Omega} - 2e^{-2x/\Omega} + e^{-3/\Omega}) \delta g \\ &= \Omega(3 \ln 2 - \ln 3 - C + \ln \Omega) \\ E[10 \log_{10} g] &= \alpha(3 \ln 2 - \ln 3 - C) + \mu_\Omega \\ &= \mu_G. \end{aligned} \quad (B.5)$$

Similarly, the second moment of the approximation is

$$\begin{aligned} E[(10 \log_{10} g)^2] &= \int_0^\infty \int_0^\infty (10 \log_{10} g)^2 \frac{3}{\Omega} e^{-g/\Omega} (1 - e^{-g/\Omega})^2 \\ &\quad \times \frac{\alpha}{\sqrt{2\pi}\sigma_{shadow}\Omega} \exp\left(-\frac{(10 \log_{10} \Omega - \mu_\Omega)^2}{2\sigma_{shadow}^2}\right) \delta g \delta \Omega \\ &= \frac{\alpha^2}{\Omega} \int_0^\infty \frac{\alpha}{\sqrt{2\pi}\sigma_{shadow}\Omega} \exp\left(-\frac{(10 \log_{10} \Omega - \mu_\Omega)^2}{2\sigma_{shadow}^2}\right) \\ &\quad \times \int_0^\infty 3(\ln g)^2 (e^{-x/\Omega} - 2e^{-2x/\Omega} + e^{-3/\Omega}) \delta g \delta \Omega. \end{aligned} \quad (B.6)$$

According to [18, (4.358.2)]

$$\begin{aligned} &\int_0^\infty 3(\ln g)^2 (e^{-x/\Omega} - 2e^{-2x/\Omega} + e^{-3/\Omega}) \delta g \\ &= \Omega[-6C \ln 2 + 6 \ln 2 \ln \Omega - 3(\ln 2)^2 + C^2 - 2C \ln \Omega \\ &\quad + (\ln \Omega)^2 + 2C \ln 3 - 2 \ln 3 \ln \Omega + (\ln 3)^2 + \zeta(2, 1)] \\ E[(10 \log_{10} g)^2] &= \alpha^2[-6C \ln 2 - 3(\ln 2)^2 + C^2 + 2C \ln 3 \\ &\quad + (\ln 3)^2 + \zeta(2, 1)] \\ &\quad + 6 \ln 2 \mu_\Omega - 2C \mu_\Omega - 2 \ln 3 \mu_\Omega + \sigma_{shadow}^2 + \mu_\Omega^2. \quad (B.7) \end{aligned}$$

Therefore, the variance of the log-normal approximation is

$$\begin{aligned} \sigma_G^2 &= E[(10 \log_{10} g)^2] - \mu_G^2 \\ &= \alpha^2[\zeta(2, 1) - 12(\ln 2)^2 + 6 \ln 2 \ln 3] + \sigma_{shadow}^2 \quad (B.8) \end{aligned}$$

#### REFERENCES

- [1] J. Shapira, "Microcell engineering in CDMA cellular networks," *IEEE Trans. Veh. Technol.*, vol. 43, pp. 817–825, Nov. 1994.
- [2] J. S. Wu, J. K. Chung, and Y. C. Yang, "Performance improvement for a hotspot embedded in CDMA system," in *Proc. Veh. Technol. Conf.*, Atlanta, GA, May 1996, pp. 944–948.
- [3] D. D. Lee, D. H. Kim, Y. J. Chung, H. G. Kim, and K. C. Whang, "Other-cell interference with power control in macro/microcell CDMA networks," in *Proc. Veh. Technol. Conf.*, Atlanta, GA, May 1996, pp. 1120–1124.
- [4] S. V. Hanly, "Capacity and power control in spread spectrum macrodiversity radio networks," *IEEE Trans. Commun.*, vol. 44, pp. 247–256, Feb. 1996.
- [5] J.-L. Gorricho, A. Rojas, and J. Paradells, "Power control at the combiner output to maximize the uplink capacity on a cellular spread spectrum system," *IEEE Commun. Lett.*, vol. 2, pp. 273–275, Oct. 1998.
- [6] K. Hamabe, S. Yoshida, and A. Ushirokawa, "Forward-link power control utilizing neighboring-cell pilot power for DS-CDMA cellular systems," in *Proc. Veh. Technol. Conf.*, Phoenix, AZ, May 1997, pp. 939–943.
- [7] K. Rohani, M. Harrison, and K. Kuchi, "A comparison of base station transmit diversity methods for third generation cellular standards," presented at the Veh. Technol. Conf., Houston, TX, May 1999.
- [8] M. Raitola, A. Hottinen, and R. Wichman, "Transmission diversity in wideband CDMA," presented at the Veh. Technol. Conf., Houston, TX, May 1999.

- [9] R. R. Gejji, "Forward-link power control in CDMA cellular systems," *IEEE Trans. Veh. Technol.*, vol. 43, pp. 532–236, Nov. 1992.
- [10] M. Zorzi, "Simplified forward-link power control law in cellular CDMA," *IEEE Trans. Veh. Technol.*, vol. 43, pp. 532–236, Nov. 1994.
- [11] G. L. Stüber, *Principles of Mobile Communication*. Norwell, MA: Kluwer, 1996.
- [12] R. D. Yates, "A framework for uplink power control in cellular radio system," *IEEE J. Select. Areas Commun.*, vol. 13, pp. 1341–1347, Sept. 1995.
- [13] M. Zorzi, "On the analytical computation of the interference statistics with applications to the performance evaluation of mobile radio systems," *IEEE Trans. Commun.*, vol. 45, pp. 103–109, Jan. 1997.
- [14] S. M. Alamouti, "A simple transmit diversity technique for wireless communications," *IEEE J. Select. Areas Commun.*, vol. 16, pp. 1451–1458, Oct. 1998.
- [15] H. Yanikomeroglu and E. S. Sousa, "CDMA sectorized distributed antenna system," in *Proc. IEEE ISSSTA*, Sun City, South Africa, Sept. 1998, pp. 792–797.
- [16] R. Sabella, "Performance analysis of wireless broadband systems employing optical fiber links," *IEEE Trans. Commun.*, vol. 47, pp. 715–721, May 1999.
- [17] A. Hottinen and R. Wichman, "Transmit diversity by antenna selection in CDMA downlink," in *IEEE ISSSTA'98*, Sun City, South Africa, Sept. 1998, pp. 792–797.
- [18] I. S. Gradshteyn, I. M. Ryzhik, and A. Jeffrey, *Table of Integrals, Series, and Products*, 5th ed. San Diego, CA: Academic, 1994.



**John Y. Kim** (S'97) received the B.S. degree in electrical engineering (with honors) from Carnegie Mellon University, Pittsburgh, PA, in 1993 and the M.S. degree in electrical engineering from the University of Michigan, Ann Arbor, in 1994. Since the fall of 1997, he has been working toward the Ph.D. degree at the School of Electrical and Computer Engineering, Georgia Institute of Technology, Atlanta.

From 1994 to 1997, he was a Project Manager at SOTAS, Inc., Gaithersburg, MD, where he was involved in developing and integrating telecommunications monitoring and diagnostic systems. His main research interest is focused on resource management issues in current and future wireless cellular systems.



**Gordon L. Stüber** (S'81–M'82–SM'96–F'99) received the B.A.Sc. and Ph.D. degrees in electrical engineering from the University of Waterloo, Waterloo, ON, Canada, in 1982 and 1986, respectively.

Since 1986, he has been with the School of Electrical and Computer Engineering, Georgia Institute of Technology, Atlanta, where he is currently a Professor. He is also Vice President for Research with WiLAN, Inc. His research interests are in wireless communications and communication signal processing. He is author of the textbook *Principles of Mobile Communication* (Norwell, MA: Kluwer, 2nd ed., 2000).

Dr. Stüber was co-recipient of the "Jack Neubauer Memorial Award" for the best paper of the year published by the IEEE Vehicular Technology Society on the subject of Vehicular Technology Systems. He served as Technical Program Chair for the 1996 IEEE Vehicular Technology Conference (VTC'96) and Technical Program Chair for the 1998 IEEE International Conference on Communications (ICC'98), and Chair of the 2000 IEEE Workshop on Multimedia, Multiaccess, and Teletraffic for Wireless Communications. He is a past Editor for Spread Spectrum with the IEEE TRANSACTIONS ON COMMUNICATIONS (1993–1998). He is currently a member of the IEEE Communication Society Awards Committee, the IEEE Vehicular Technology Society Board of Governors, Chair of the 2002 Communication Theory Workshop, and Chair of the Fifth YRP International Symposium.



**Ian F. Akyildiz** (M'86–SM'89–F'95) is a Distinguished Chair Professor with the School of Electrical and Computer Engineering, Georgia Institute of Technology, Atlanta, and Director of Broadband and Wireless Networking Laboratory. His current research interests are in wireless networks, satellite networks, and the Internet.

Dr. Akyildiz is the Editor-in-Chief of the *Computer Networks* (Elsevier) and an Editor for IEEE/ACM TRANSACTIONS ON NETWORKING, ACM-Springer Journal for Multimedia Systems, ACM-Baltzer Journal of Wireless Networks, and Journal of Cluster Computing. He is a past Editor for IEEE TRANSACTIONS ON COMPUTERS (1992–1996). He was the Program Chair of the "9th IEEE Computer Communications" workshop, held in Florida in October 1994. He also served as the Program Chair for ACM/IEEE MOBICOM'96 (Mobile Computing and Networking) conference, as well as for the IEEE INFOCOM'98 conference. He will be the General Chair for ACM/IEEE Mobicom 2002 conference and Technical Program Chair of IEEE ICC 2003. He is an ACM Fellow (1996). He received the "Don Federico Santa Maria Medal" for his services to the Universidad Federico Santa Maria in Chile. He served as a National Lecturer for ACM from 1989 until 1998 and received the ACM Outstanding Distinguished Lecturer Award for 1994. He received the 1997 IEEE Leonard G. Abraham Prize award for his paper entitled "Multimedia Group Synchronization Protocols for Integrated Services Architectures," published in the IEEE JOURNAL ON SELECTED AREAS IN COMMUNICATIONS in January 1996.